Am J Physiol Heart Circ Physiol 282: H516–H530, 2002.
First published October 4, 2001; 10.1152/ajpheart.00612.2001.

Ionic mechanism of electrical alternans

JEFFREY J. FOX,[1,2] JENNIFER L. McHARG,[1] AND ROBERT F. GILMOUR, JR[1]
[1]*Department of Biomedical Sciences and* [2]*Department of Physics, Cornell University, Ithaca, New York 14853-6401*

Received 12 July 2001; accepted in final form 26 September 2001

Fox, Jeffrey J., Jennifer L. McHarg, and Robert F. Gilmour, Jr. Ionic mechanism of electrical alternans. *Am J Physiol Heart Circ Physiol* 282: H516–H530, 2002. First published October 4, 2001; 10.1152/ajpheart.00612.2001.—Although alternans of action potential duration (APD) is a robust feature of the rapidly paced canine ventricle, currently available ionic models of cardiac myocytes do not recreate this phenomenon. To address this problem, we developed a new ionic model using formulations of currents based on previous models and recent experimental data. Compared with existing models, the inward rectifier K^+ current (I_{K1}) was decreased at depolarized potentials, the maximum conductance and rectification of the rapid component of the delayed rectifier K^+ current (I_{Kr}) were increased, and I_{Kr} activation kinetics were slowed. The slow component of the delayed rectifier K^+ current (I_{Ks}) was increased in magnitude and activation shifted to less positive voltages, and the L-type Ca^{2+} current (I_{Ca}) was modified to produce a smaller, more rapidly inactivating current. Finally, a simplified form of intracellular calcium dynamics was adopted. In this model, APD alternans occurred at cycle lengths = 150–210 ms, with a maximum alternans amplitude of 39 ms. APD alternans was suppressed by decreasing I_{Ca} magnitude or calcium-induced inactivation and by increasing the magnitude of I_{K1}, I_{Kr}, or I_{Ks}. These results establish an ionic basis for APD alternans, which should facilitate the development of pharmacological approaches to eliminating alternans.

action potential duration restitution; calcium current; potassium currents

THE DURATION of the cardiac action potential is determined in large part by the preceding diastolic interval. This relationship between action potential duration and diastolic interval, known as the action potential duration restitution relation, is an important determinant of cardiac dynamics (17). In particular, if the slope of the restitution relation is ≥ 1, an alternation of action potential duration, or electrical alternans, commonly develops during high-frequency pacing (2, 8).

It has been suggested that rate-dependent electrical alternans may be a precursor to the development of ventricular arrhythmias, particularly ventricular fibrillation (VF) (6, 10, 19, 22). In support of this idea, several recent experiments (5, 11, 23) have shown that when the slope of the restitution relation is ≥ 1, rapid pacing induces both alternans and fibrillation in isolated ventricles. If the slope of the restitution relation is reduced to <1, neither electrical alternans nor fibrillation occurs (5, 11, 12, 23). Unfortunately, the interventions used to date to suppress alternans and fibrillation [high-dose calcium channel blockers (23), hyperkalemia (12), and bretylium (5)] have limited clinical utility. More effective means of suppressing alternans need to be identified, a process that would be facilitated by a more complete understanding of the ionic basis for alternans.

One approach to determining the ionic basis for alternans is to use a computer model, several of which have been developed. For example, Luo and Rudy (15, 16), using data obtained primarily from guinea pig myocytes, developed a comprehensive ionic model (LR1) that subsequently was updated (LRd) to include formulations for the rapid and slow components of the delayed rectifier K^+ current (I_{Kr} and I_{Ks}, respectively). Recently, Winslow et al. (26) modified the LRd model using data for ionic currents obtained from canine ventricular myocytes (CVM) and a formulation for calcium dynamics developed originally in guinea pig myocardial cells (9). An alternative formulation for calcium dynamics has been proposed by Chudin et al. (1) in their modification of the LR1 model.

Each of the models described above has limitations with respect to the study of the ionic basis for electrical alternans. The Winslow and LRd models do not produce sustained alternans at rapid pacing rates, whereas the Chudin model, which does generate electrical alternans, lacks formulations for repolarizing K^+ currents likely to contribute importantly to alternans [I_{Kr}, I_{Ks}, and the transient outward K^+ current (I_{to})].

Given that a complete ionic model that generates electrical alternans is not currently available, we set out to develop such a model, guided by the results obtained from our experimental studies in the canine ventricle (11, 23). Our initial objectives were to develop an ionic model of the CVM that exhibits stable electrical alternans and to use the model to identify the ionic currents responsible for alternans. Once the relevant ionic currents were identified, we then manipulated these currents to eliminate alternans. Our expectation is that the same ionic manipulations that suppress alternans in the ionic model will suppress fibrillation

Address for reprint requests and other correspondence: R. F. Gilmour, Jr., Dept. of Biomedical Sciences, T7 012C VRT, Cornell Univ., Ithaca, NY 14853-6401 (E-mail: rfg2@cornell.edu).

The costs of publication of this article were defrayed in part by the payment of page charges. The article must therefore be hereby marked "*advertisement*" in accordance with 18 U.S.C. Section 1734 solely to indicate this fact.

in vivo, in which case the results of the present study may suggest novel approaches to the prevention of VF.

Glossary

α_h	Voltage-dependent h gate parameter
α_j	Voltage-dependent j gate parameter
α_m	Voltage-dependent m gate parameter
$\alpha_{X_{to}}$	Voltage-dependent X_{to} gate parameter
β_h	Voltage-dependent h gate parameter
β_i	Myoplasmic buffering factor
β_j	Voltage-dependent j gate parameter
β_m	Voltage-dependent m gate parameter
β_{SR}	Sarcoplasmic reticulum buffering factor
$\beta_{X_{to}}$	Voltage-dependent X_{to} gate parameter
γ	Sarcoplasmic reticulum Ca^{2+}-dependent J_{rel} factor
η	Controls voltage dependence of I_{NaCa}
σ	Extracellular Na^+ I_{NaK} factor
τ_d	I_{Ca} activation time constant
τ_f	I_{Ca} inactivation time constant
$\tau_{f_{Ca}}$	Ca^{2+}-dependent I_{Ca} inactivation time constant
τ_{Kr}	I_{Kr} activation time constant
τ_{Ks}	I_{Ks} activation time constant
A_{cap}	Capacitive membrane area
APD	Action potential duration
BCL	Basic cycle length
C_{sc}	Specific membrance capacity
ΔCa_{max}	Maximum change in Ca^{2+}
ΔCa_{min}	Minimum change in Ca^{2+}
$[Ca^{2+}]_i$	Intracellular Ca^{2+} concentration
$[Ca^{2+}]_o$	Extracellular Ca^{2+} concentration
$[Ca^{2+}]_{SR}$	Sarcoplasmic reticulum Ca^{2+} concentration
$[CMDN]_{tot}$	Total calmodulin concentration
$[CSQN]_{tot}$	Total calsequestrin concentration
CVM	Canine ventricular myocyte
d	I_{Ca} activation gate
d^∞	Steady-state I_{Ca} activation
DI	Diastolic interval
E_{Ca}	Ca^{2+} equilibrium potential
E_K	K^+ equilibrium potential
E_{Ks}	I_{Ks} equilibrium potential
E_{Na}	Na^+ equilibrium potential
f	I_{Ca} inactivation gate
f^∞	Steady-state I_{Ca} inactivation
f_{Ca}^∞	Steady-state Ca^{2+}-dependent I_{Ca} inactivation
f_{Ca}	Ca^{2+}-dependent I_{Ca} inactivation gate
f_{NaK}	Voltage-dependent I_{NaK} factor
F	Faraday constant
$\bar{G}_{Cab}$	Peak I_{Cab} conductance
$\bar{G}_{K1}$	Peak I_{K1} conductance
$\bar{G}_{Kp}$	Peak I_{Kp} conductance
$\bar{G}_{Kr}$	Peak I_{Kr} conductance
$\bar{G}_{Ks}$	Peak I_{Ks} conductance
$\bar{G}_{Na}$	Peak I_{Na} conductance
$\bar{G}_{to}$	Peak I_{to} conductance
h	Fast I_{Na} inactivation gate
I_{Ca}	L-type Ca^{2+} channel current
$\bar{I}_{Ca}$	Maximal I_{Ca}
I_{Cab}	Ca^{2+} background current
I_{Cahalf}	$\bar{I}_{Ca}$ level that reduces $\bar{P}_{CaK}$ by one-half
I_{CaK}	K^+ current through the L-type Ca^{2+} channel
I_{K1}	Inward rectifier K^+ current
I_{Kp}	Plateau K^+ current
I_{Kr}	Rapid component of the delayed rectifier K^+ current
I_{Ks}	Slow component of the delayed rectifier K^+ current
I_{Na}	Na^+ current
I_{Nab}	Na^+ background current
I_{NaCa}	Na^+/Ca^{2+} exchange current
I_{NaK}	Na^+-K^+ pump current
$\bar{I}_{NaK}$	Maximal I_{NaK}
I_{pCa}	Sarcolemmal Ca^{2+} pump current
$\bar{I}_{pCa}$	Maximal I_{pCa}
I_{stim}	Stimulus current
I_{to}	Transient outward K^+ current
j	Slow I_{Na} inactivation gate
J_{leak}	Leakage Ca^{2+} flux from the sarcoplasmic reticulum
J_{rel}	Release Ca^{2+} flux from the sarcoplasmic reticulum
J_{up}	Uptake Ca^{2+} flux to the sarcoplasmic reticulum
JSR	Junctional sarcoplasmic reticulum
k_{NaCa}	Scaling factor for I_{NaCa}
k_{sat}	I_{NaCa} saturation factor for I_{NaCa}
K_1^∞	Steady-state I_{K1} activation
K_{Kp}	I_{Kp} activation
K_m^{CMDN}	Ca^{2+} half-saturation constant for calmodulin
K_m^{CSQN}	Ca^{2+} half-saturation constant for calsequestrin
K_{mCa}	Ca^{2+} half-saturation constant for I_{NaCa}
$K_{mf_{Ca}}$	Ca^{2+} half-saturation constant for f_{Ca}
K_{mK1}	K^+ half-saturation constant for I_{K1}
K_{mKo}	K^+ half-saturation constant for I_{NaK}
K_{mNa}	Na^+ half-saturation constant for I_{NaCa}
K_{mNai}	Na^+ half-saturation constant for I_{NaK}
K_{mpCa}	Half-saturation constant for I_{pCa}
K_{mup}	Ca^{2+} half-saturation constant for J_{up}
$[K^+]_i$	Intracellular K^+ concentration
$[K^+]_o$	Extracellular K^+ concentration
LR1	Luo and Rudy model
LRd	Updated Luo and Rudy model
m	I_{Na} activation gate
$[Na^+]_i$	Intracellular Na^+ concentration
$[Na^+]_o$	Extracellular Na^+ concentration
NSR	Nonjunctional sarcoplasmic reticulum
$\bar{P}_{Ca}$	L-type Ca^{2+} channel permeability to Ca^{2+}
$\bar{P}_{CaK}$	L-type Ca^{2+} channel permeability to K^+
$\bar{P}_{leak}$	Ca^{2+} leakage permability between the sarcoplasmic reticulum and the myoplasm
$\bar{P}_{rel}$	Ca^{2+} maximal release permeability from the sarcoplasmic reticulum
R	Ideal gas constant

SR	Sarcoplasmic reticulum
t	Time
T	Temperature
V	Voltage
ΔV_{max}	Maximum change in voltage
ΔV_{min}	Minimum change in voltage
V_{myo}	Myoplasmic volume
V_{SR}	Sarcoplasmic reticulum volume
V_{up}	Maximal Ca^{2+} uptake to the sarcoplasmic reticulum
VF	Ventricular fibrillation
X_{Kr}	I_{Kr} activation gate
X_{Kr}^{∞}	Steady-state I_{Kr} activation
X_{Ks}	I_{Ks} activation gate
X_{Ks}^{∞}	Steady-state I_{Ks} activation
X_{to}	I_{to} activation gate
Y_{to}	I_{to} inactivation gate

MATERIALS AND METHODS

To study the ionic mechanism of electrical alternans in canine myocytes, we constructed a CVM model using appropriate formulations of ionic currents from the LRd, Winslow, and Chudin models, altered as necessary to fit experimental voltage-clamp data from CVM. It has been well established that cellular electrical properties in the canine ventricle vary, both between right and left ventricles and within a given ventricle, according to whether a cell resides in the epicardium, endocardium, or midmyocardium (13, 14). Because the Winslow model is the only existing ionic model based on the electrical properties of the canine ventricle, we elected to use that model as the basis for the CVM model. Consequently, the CVM model, like its predecessor, recreates the midmyocardial or M cell action potential. Further alterations of various currents, including I_{Ks}, I_{to} and I_{NaCa}, would be required to model the electrical activity of canine endocardial and epicardial myocytes (13, 29).

The CVM model contains the following ionic current formulations

$$\frac{dV}{dt} = -(I_{stim} + I_{Na} + I_{Kl} + I_{Kr} + I_{Ks} + I_{to} + I_{Kp} + I_{NaK} + I_{NaCa} + I_{Nab} + I_{Cab} + I_{pCa} + I_{Ca} + I_{CaK})$$

Stimulus current. I_{stim} used to drive the model was a square wave pulse consisting of -80 μA/μF of current for 1 ms.

Sodium current. I_{Na} was the same as that used in the Winslow model (26) except that the discontinuities in the h and j gate formulations were removed.

$$I_{Na} = \bar{G}_{Na} m^3 h j (V - E_{Na})$$

$$\frac{dm}{dt} = \alpha_m(1 - m) - \beta_m m$$

$$\frac{dh}{dt} = \alpha_h(1 - h) - \beta_h h$$

$$\frac{dj}{dt} = \alpha_j(1 - j) - \beta_j j$$

$$E_{Na} = \frac{RT}{F} \ln\left(\frac{[Na^+]_o}{[Na^+]_i}\right)$$

$$\alpha_m = 0.32 \frac{V + 47.13}{1 - e^{-0.1(V + 47.13)}}$$

$$\beta_m = 0.08 e^{-V/11}$$

$$\alpha_h = 0.135 e^{(V+80)/-6.8}$$

$$\beta_h = \frac{7.5}{1 + e^{-0.1(V + 11)}}$$

$$\alpha_j = \frac{0.175 e^{(V+100)/-23}}{1 + e^{0.15(V + 79)}}$$

$$\beta_j = \frac{0.3}{1 + e^{-0.1(V + 32)}}$$

Inward rectifier K^+ current. I_{K1} was formulated to agree with data from Freeman et al. (4). These data indicate a smaller outward current at depolarized potentials than is seen in the Winslow model

$$I_{K1} = \bar{G}_{K1} K_1^{\infty} \frac{[K^+]_o}{[K^+]_o + K_{mK1}} (V - E_K)$$

$$K_1^{\infty} = \frac{1}{2 + e^{1.62F/(RT)(V - E_K)}}$$

$$E_K = \frac{RT}{F} \ln\left(\frac{[K^+]_o}{[K^+]_i}\right)$$

Rapid component of the delayed rectifier K^+ current. I_{Kr} was fit to the data from Gintant (7). In particular, we reproduced the voltage-clamp experiment used to generate Fig. 2 in his paper. The Winslow formulation of the current was altered to increase rectification, slow kinetics at depolarized potentials, and increase maximum conductance

$$I_{Kr} = \bar{G}_{Kr} R(V) X_{Kr} \sqrt{\frac{[K^+]_o}{4}} (V - E_K)$$

$$\frac{dX_{Kr}}{dt} = \frac{X_{Kr}^{\infty} - X_{Kr}}{\tau_{Kr}}$$

$$R(V) = \frac{1}{1 + 2.5 e^{0.1(V + 28)}}$$

$$\tau_{Kr} = 43 + \frac{1}{e^{-5.495 + 0.1691V} + e^{-7.677 - 0.0128V}}$$

$$X_{Kr}^{\infty} = \frac{1}{1 + e^{-2.182 - 0.1819V}}$$

Slow component of the delayed rectifier K^+ current. I_{Ks} was fit to data from Varro et al. (25), specifically the results shown in Fig. 2 of their paper. The Winslow model was altered to increase the magnitude of the current and shift activation to less positive voltages

$$I_{Ks} = \bar{G}_{Ks} X_{Ks}^2 (V - E_{Ks})$$

$$E_{Ks} = \frac{RT}{F} \ln\left(\frac{[K^+]_o + 0.01833[Na^+]_o}{[K^+]_i + 0.01833[Na^+]_i}\right)$$

$$\frac{dX_{Ks}}{dt} = \frac{X_{Ks}^{\infty} - X_{Ks}}{\tau_{Ks}}$$

$$X_{Ks}^{\infty} = \frac{1}{1 + e^{(V-16)/-13.6}}$$

$$\tau_{Ks} = \frac{1}{\frac{0.0000719(V - 10)}{1 - e^{-0.148(V - 10)}} + \frac{0.000131(V - 10)}{e^{0.0687(V - 10)} - 1}}$$

Transient outward K^+ current. I_{to} in the model was the same as that in the Winslow model

$$I_{to} = \bar{G}_{to} X_{to} Y_{to} (V - E_K)$$

$$\frac{dX_{to}}{dt} = \alpha_{X_{to}}(1 - X_{to}) - \beta_{X_{to}} X_{to}$$

$$\frac{dY_{to}}{dt} = \alpha_{Y_{to}}(1 - Y_{to}) - \beta_{Y_{to}} Y_{to}$$

$$\alpha_{X_{to}} = 0.04516 e^{0.03577V}$$

$$\beta_{X_{to}} = 0.0989 e^{-0.06237V}$$

$$\alpha_{Y_{to}} = \frac{0.005415 e^{(V+33.5)/-5}}{1 + 0.051335 e^{(V+33.5)/-5}}$$

$$\beta_{Y_{to}} = \frac{0.005415 e^{(V+33.5)/5}}{1 + 0.051335 e^{(V+33.5)/5}}$$

Plateau K^+ current. I_{Kp} was the same as that in the Winslow model

$$I_{Kp} = \bar{G}_{Kp} K_{Kp}(V - E_K)$$

$$K_{Kp} = \frac{1}{1 + e^{(7.488 - V)/5.98}}$$

Na^+-K^+ pump current. I_{NaK} was the same as that in the LRd model

$$I_{NaK} = \bar{I}_{NaK} f_{NaK} \frac{1}{1 + \left(\frac{K_{mNai}}{[Na^+]_i}\right)^{1.5}} \frac{[K^+]_o}{[K^+]_o + K_{mKo}}$$

$$f_{NaK} = \frac{1}{1 + 0.1245e^{-0.1VF/(RT)} + 0.0365\sigma e^{-VF/(RT)}}$$

$$\sigma = 1/7\ (e^{[Na^+]_o/67.3} - 1)$$

Na^+/Ca^{2+} exchange current, sarcolemmal pump current, and Ca^{2+} and Na^+ background currents. I_{NaCa}, I_{pCa}, I_{Cab}, and I_{Nab} were the same as those in the Winslow model

$$I_{Nab} = \bar{G}_{Nab}(V - E_{Na})$$

$$I_{NaCa} = \frac{k_{NaCa}}{K_{mNa}^3 + [Na^+]_o^3} \frac{1}{K_{mCa} + [Ca^{2+}]_o} \frac{1}{1 + k_{sat} e^{VF(\eta - 1)/(RT)}} \times [e^{VF\eta/(RT)}[Na^+]_i^3[Ca^{2+}]_o - e^{VF(\eta-1)/(RT)}[Na^+]_o^3[Ca^{2+}]_i]$$

$$I_{pCa} = \bar{I}_{pCa} \frac{[Ca^{2+}]_i}{K_{mpCa} + [Ca^{2+}]_i}$$

$$I_{Cab} = \bar{G}_{Cab}(V - E_{Ca})$$

$$E_{Ca} = \frac{RT}{2F} \ln\left(\frac{[Ca^{2+}]_o}{[Ca^{2+}]_i}\right)$$

L-type Ca^{2+} channel current. I_{Ca} in the model was a modified version of that found in the LRd model. A time-dependent, enhanced Ca^{2+}-induced inactivation was used, as well as a decrease in the current magnitude. These changes produced a smaller, more rapidly inactivating Ca^{2+} current, in agreement with experimental observations by A. C. Zygmunt (personal communication)

$$I_{Ca} = \bar{I}_{Ca} f d f_{Ca}$$

$$\bar{I}_{Ca} = \frac{\bar{P}_{Ca}}{C_{sc}} \frac{4VF^2}{RT} \frac{[Ca^{2+}]_i e^{2VF/(RT)} - 0.341[Ca^{2+}]_o}{e^{2VF/(RT)} - 1}$$

$$\frac{df}{dt} = \frac{f^\infty - f}{\tau_f}$$

$$\frac{dd}{dt} = \frac{d^\infty - d}{\tau_d}$$

$$\frac{df_{Ca}}{dt} = \frac{f_{Ca}^\infty - f_{Ca}}{\tau_{f_{Ca}}}$$

$$f^\infty = \frac{1}{1 + e^{(V + 12.5)/5}}$$

$$\tau_f = 30 + \frac{200}{1 + e^{(V+20)/9.5}}$$

$$d^\infty = \frac{1}{1 + e^{(V+10)/-6.24}}$$

$$\tau_d = \frac{1}{\frac{0.25e^{-0.01V}}{1 + e^{-0.07V}} + \frac{0.07e^{-0.05(V+40)}}{1 + e^{0.05(V+40)}}}$$

$$f_{Ca}^\infty = \frac{1}{1 + \left(\frac{[Ca^{2+}]_i}{K_{mf_{Ca}}}\right)^3}$$

$$\tau_{f_{Ca}} = 30$$

K^+ current through the L-type Ca^{2+} channel. I_{CaK} was also a modified version of the LRd formulation

$$I_{CaK} = \frac{\bar{P}_{CaK}}{C_{sc}} \frac{f d f_{Ca}}{1 + \frac{\bar{I}_{Ca}}{I_{Cahalf}}} \frac{1{,}000VF^2}{RT} \frac{[K^+]_i e^{VF/(RT)} - [K^+]_o}{e^{VF/(RT)} - 1}$$

Calcium handling. A modified form of the intracellular calcium dynamics from Chudin et al. (1) was used. We included buffering from calmodulin in the cytoplasm and calsequestrin in the SR, omitted spontaneous release of calcium from the SR, and combined the concentrations of calcium in the JSR and NSR into a single variable

$$\frac{d[Ca^{2+}]_i}{dt} = \beta_i \left(J_{rel} + J_{leak} - J_{up} - \frac{A_{Cap} C_{sc}}{2FV_{myo}} \times (I_{Ca^+} I_{Cab} + I_{pCa} - 2I_{NaCa}) \right)$$

$$\beta_i = \left(1 + \frac{[CMDN]_{tot} K_m^{CMDN}}{(K_m^{CMDN} + [Ca^{2+}]_i)^2}\right)^{-1}$$

$$J_{rel} = \bar{P}_{rel} f d f_{Ca} \frac{\gamma[Ca^{2+}]_{SR} - [Ca^{2+}]_i}{1 + 1.65e^{V/20}}$$

$$\gamma = \frac{1}{1 + \left(\frac{2{,}000}{[Ca^{2+}]_{SR}}\right)^3}$$

$$J_{up} = \frac{V_{up}}{1 + \left(\frac{K_{m_{up}}}{[Ca^{2+}]_i}\right)^2}$$

$$J_{leak} = \bar{P}_{leak}([Ca^{2+}]_{SR} - [Ca^{2+}]_i)$$

$$\frac{d[Ca^{2+}]_{SR}}{dt} = \beta_{SR}(J_{up} - J_{leak} - J_{rel}) \frac{V_{myo}}{V_{SR}}$$

$$\beta_{SR} = \left(1 + \frac{[CSQN]_{tot} K_m^{CSQN}}{(K_m^{CSQN} + [Ca^{2+}]_{SR})^2}\right)^{-1}$$

Numerical methods. The equations listed above were solved using parameter values and initial conditions found in Table 1. The simulations were run on Macintosh G3 and G4 computers using a program written in C. The numerical integration scheme was similar to that used in Luo and Rudy (15, 16) and in Rush and Larsen (24). Briefly, the time steps of integration were made small enough so that the changes in voltage and in calcium concentrations remained below maximum values, ΔV_{max} and ΔCa_{max}. If the changes in voltage and calcium concentration were below a minimum value (ΔV_{min} and ΔCa_{min}), the time step was increased. By keeping the changes in voltage small, we could solve the linear gate variable equations exactly during each time step. We used the following values: ΔV_{max} = 0.8 mV, ΔV_{min} = 0.2 mV, $\Delta Ca_{max} = 1.067 \times 10^{-2}$ μM, and $\Delta Ca_{min} = 2.67 \times 10^{-3}$ μM. (See Refs. 15, 16, and 24 for more details.) The other time-dependent variables in the model were solved using the adaptive fourth-order Runge-Kutta method (21). The errors were normalized as described in Jafri et al. (9). We used a maximum error of 1×10^{-6}, a minimum time step of 0.005 ms, and a maximum time step of 0.5 ms. During the stimulus, the step size was fixed at 0.005 ms.

To further increase computational speed, lookup tables were used to avoid repeatedly calculating exponentials and other computationally expensive functions. The lookup tables were calculated once before each simulation for 15,000 values

Table 1. *Parameters and initial conditions*

	Values
Parameters	
$\bar{G}_{Na}$, mS/μF	12.8
$\bar{G}_{K1}$, mS/μF	2.8
$\bar{G}_{Kr}$, mS/μF	0.0136
$\bar{G}_{Ks}$, mS/μF	0.0245
$\bar{G}_{Kp}$, mS/μF	0.002216
$\bar{G}_{to}$, mS/μF	0.23815
$\bar{G}_{Nab}$, mS/μF	0.0031
$\bar{G}_{cab}$, mS/μF	0.0003842
$\bar{P}_{Ca}$, cm/ms	0.0000226
$\bar{P}_{CaK}$, cm/ms	5.79×10^{-7}
$\bar{P}_{rel}$, ms^{-1}	6
$\bar{P}_{leak}$, ms^{-1}	0.000001
$\bar{I}_{NaK}$, μA/μF	0.693
$\bar{I}_{Cahalf}$, μA/μF	−0.265
$\bar{I}_{pCa}$, μA/μF	0.05
R, J/mol K	8.314
T, Kelvins	310
F, coulomb/mol K	96.5
A_{cap}, cm^2	1.534×10^{-4}
C_{sc}, μF/cm^2	1
η	0.35
k_{sat}	0.2
k_{NaCa}, μA/μF	1,500
$K_{mf_{Ca}}$, μM	0.18
K_{mK1}, mM	13
K_{mNa}, mM	87.5
K_{mCa}, μM	1,380
K_{mNa_i}, mM	10
K_{mKo}, mM	1.5
K_{mpCa}, μM	0.05
K_{mup}, μM	0.32
$[CMDN]_{tot}$, μM	10
$[CSQN]_{tot}$, μM	10,000
K_m^{CMDN}, μM	2
K_m^{CSQN}, μM	600
V_{up}, μM/ms	0.1
V_{myo}, μl	25.84×10^{-6}
V_{SR}, μl	2×10^{-6}
$[Na^+]_i$, mM	10
$[K^+]_i$, mM	149.4
$[Na^+]_o$, mM	138
$[K^+]_o$, mM	4
$[Ca^{2+}]_o$, μM	2,000
Initial Conditions	
t, ms	0.0
V, mV	−94.7
$[Ca^{2+}]_i$, μmol	0.0472
$[Ca^{2+}]_{SR}$, μmol	320
f	0.983
d	0.0001
m	2.4676×10^{-4}
h	0.99869
j	0.99887
f_{Ca}	0.942
X_{Kr}	0.229
X_{Ks}	0.0001
X_{to}	3.742×10^{-5}
Y_{to}	1

See *Glossary* for abbreviations.

of voltages ranging from −100 to +100 mV. Values of voltages lying between the indexes of the lookup table were calculated using linear interpolation. To check that these numerical techniques did not affect the accuracy of the simulation, simulations also were run using no lookup tables, with a maximum time step of 0.1 ms. The action potential durations throughout a pacedown from a pacing cycle length of 400 ms to a cycle length of 90 ms differed by <1% between the two simulations.

Restitution relations were generated using the procedure described in Koller et al. (11), where action potential duration was expressed as a function of the preceding diastolic interval. The magnitude of action potential duration alternans was defined as the difference in action potential duration between two consecutive action potentials. Action potential duration was measured to 95% of repolarization.

RESULTS

Action potential and ionic currents. Figure 1 illustrates the action potentials, ionic currents, and Ca^{2+} transients generated by the CVM model at a pacing cycle length of 400 ms. The action potential (Fig. 1*A*) was characterized by the familiar spike-and-dome morphology of canine midmyocardial cells. I_{Ca} (Fig. 1*B*) was of smaller magnitude and inactivated more rapidly than I_{Ca} in previous models, in agreement with the recent experimental observations of A. C. Zygmunt (private communication). The time course and magnitude of $[Ca^{2+}]_i$ (Fig. 1*D*) was similar to experimental results reported previously (1, 26), indicating that the simplified calcium handling in the CVM model generated realistic Ca^{2+} transients.

As shown in Fig. 1*F*, I_{Kr} increased significantly toward the end of plateau, in good agreement with the data from Gintant (7). In contrast, I_{Ks} was too small to contribute significantly to repolarization at this cycle length (Fig. 1*G*, note the current scale compared with Fig. 1*F*), primarily because of its very slow recovery from deactivation (25).

Electrical alternans. The CVM model generated electrical alternans at physiologically relevant pacing cycle lengths. Figure 2 shows the action potential and selected plateau currents at a cycle length of 180 ms, where the CVM model produced stable alternans of large magnitude. Note that I_{Ca}, f_{Ca}, and the Ca^{2+} transient were significantly different between the long and short action potentials, whereas peak I_{Kr} and peak inward I_{NaCa} were not. I_{Ks} varied in magnitude between the long and short action potentials, but the peak current magnitude remained small.

Figure 3 shows the relationship between action potential duration and the pacing cycle length over the range of cycle lengths that produced electrical alternans (400–90 ms; Fig. 3*A*) and over a wider range of cycle lengths (8,000–90 ms; Fig. 3*C*). Action potentials generated at several different pacing cycle lengths are shown in Fig. 3*D*. The model generated electrical alternans over a wide range of pacing cycle lengths, in association with a region of the restitution relation having a slope equal to 1 (Fig. 3*B*). At cycle lengths <150 ms, alternans was absent. The initial increase in alternans magnitude as the pacing cycle length was shortened, followed by a subsequent decrease in alternans magnitude with a further shortening of the cycle length, is in good agreement with experimental data (11).

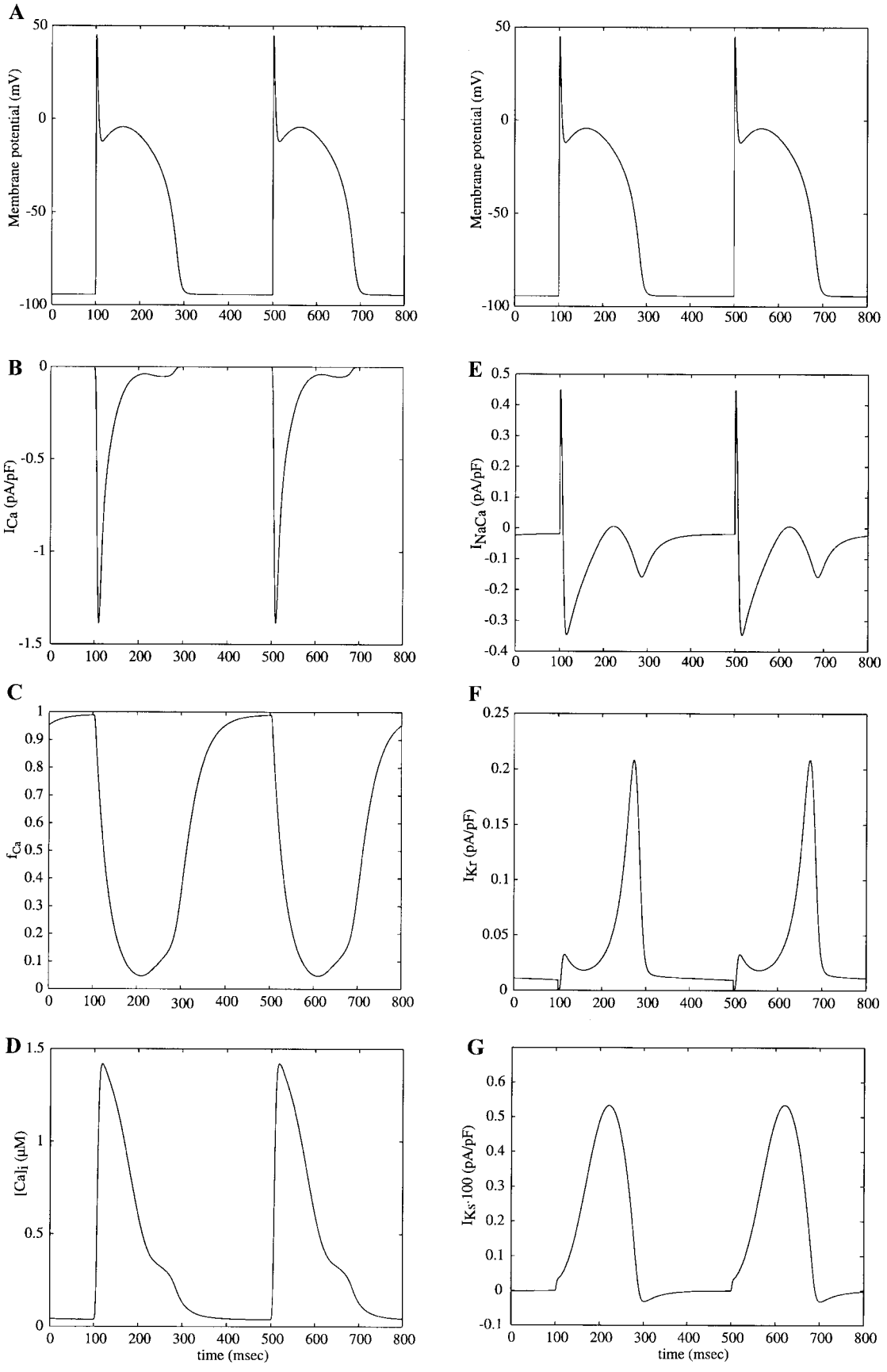

Fig. 1. Action potentials, ionic currents, and Ca^{2+} transients generated by the CVM model after 50 beats at a cycle length of 400 ms. *A*: action potentials; *B*: I_{Ca}; *C*: f_{Ca}; *D*: $[Ca^{2+}]_i$; *E*: I_{NaCa}; *F*: I_{Kr}; *G*: I_{Ks}. See *Glossary* for abbreviations.

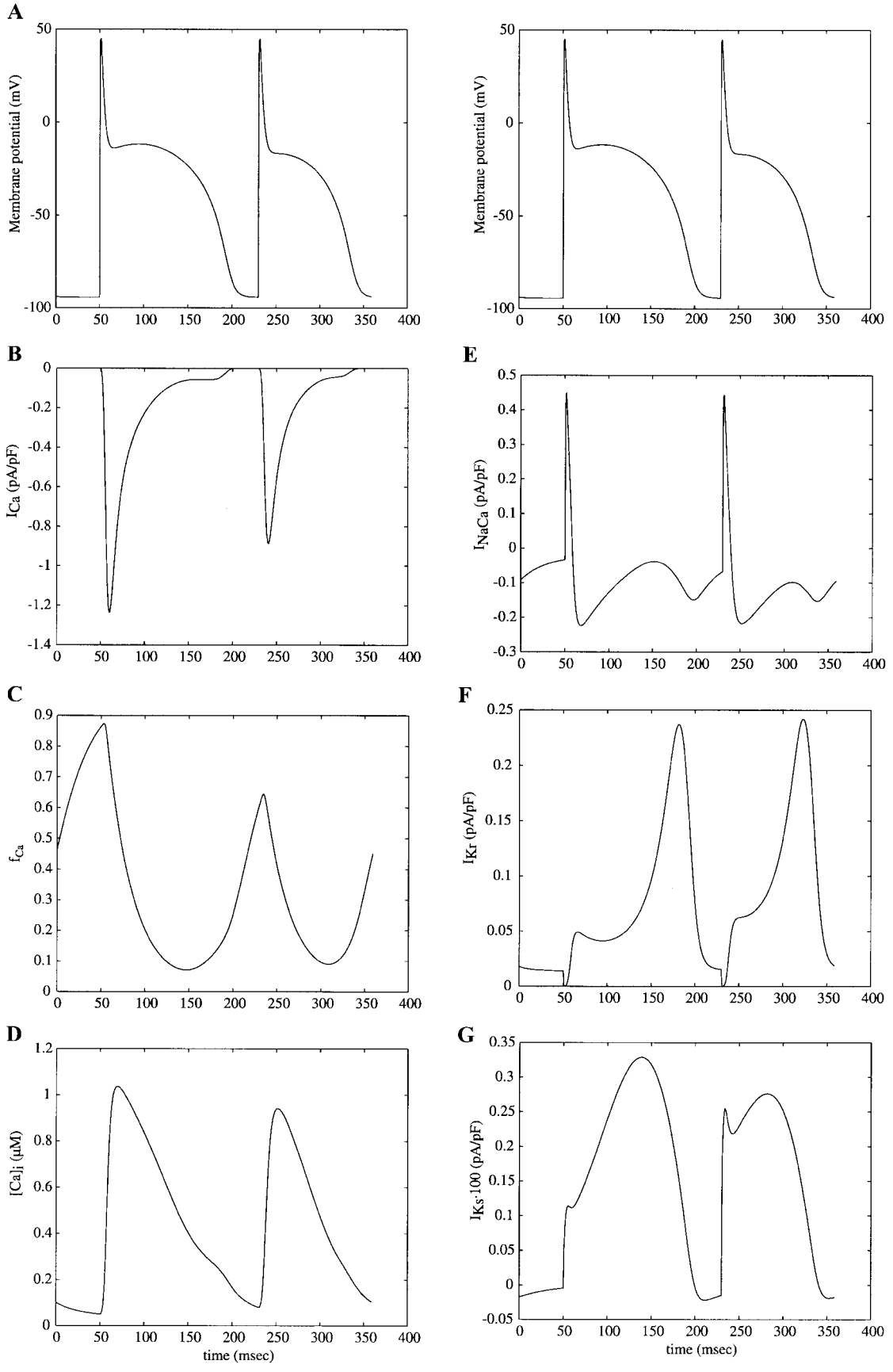

Fig. 2. Action potentials, ionic currents, and Ca^{2+} transients generated by the CVM model after 50 beats at a cycle length of 180 ms. *A*: action potentials; *B*: I_{Ca}; *C*: f_{Ca}; *D*: $[Ca^{2+}]_i$; *E*: I_{NaCa}; *F*: I_{Kr}; *G*: I_{Ks}.

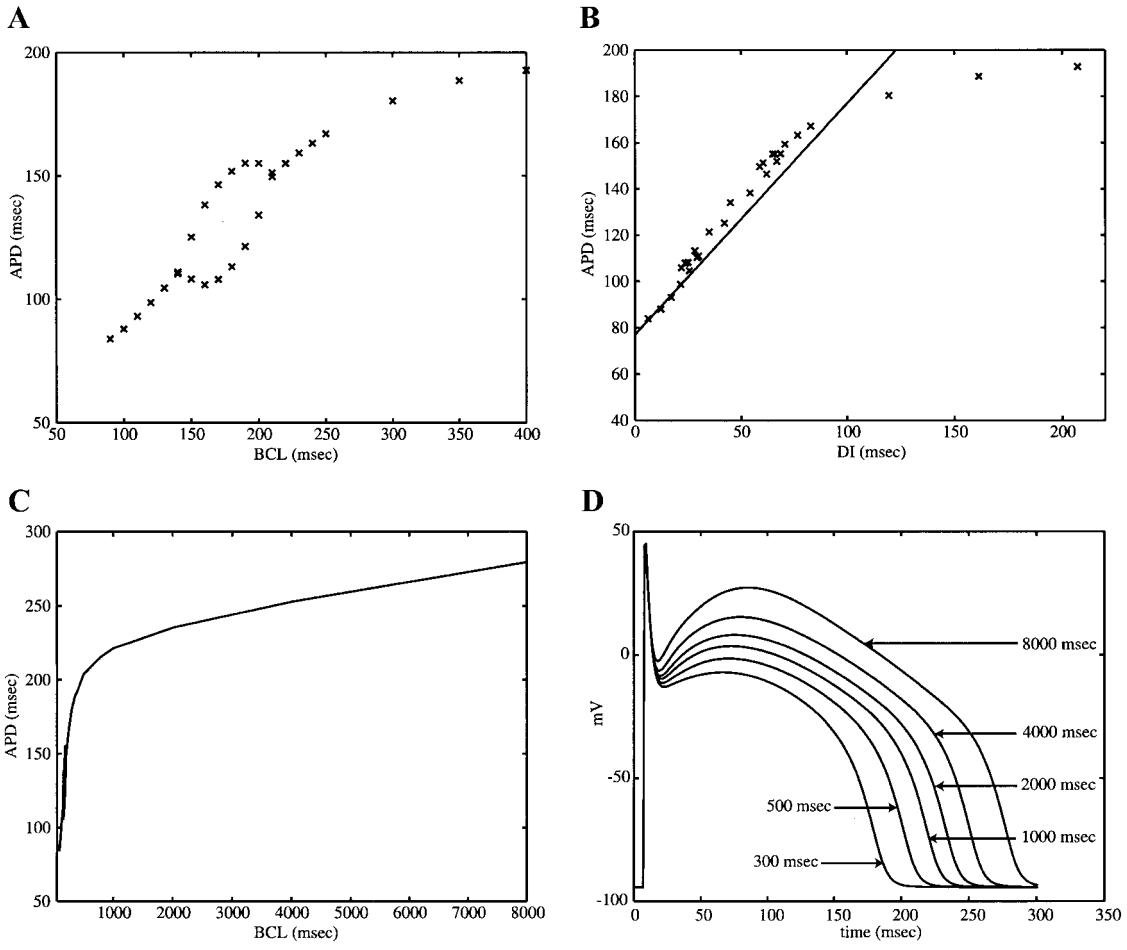

Fig. 3. Action potentials generated by the CVM model at pacing cycle lengths of 8,000–90 ms. Two-to-one block occurred at a cycle length of 80 ms. *A*: action potential duration (APD) plotted as a function of the basic cycle length (BCL) of pacing over a BCL range of 90–400 ms. *B*: APD restitution, where APD is plotted as a function of the diastolic interval (DI) for DI <210 ms. The solid line has a slope of 1. Note that alternans occurred where the slope of the restitution relation was ≥1. *C*: APD as a function of BCL over a BCL range of 90–8,000 ms. *D*: examples of action potentials at BCL = 300, 500, 1,000, 2,000, 4,000, and 8,000 ms. Over this range of BCL, resting membrane potential = −94 mV, action potential amplitude = 139 mV, overshoot = 45 mV, and maximum d*V*/d*t* = 278–280 V/s. See *Glossary* for abbreviations.

Role of plateau Na^+ and Ca^{2+} currents in alternans. The large difference in I_{Ca} between the long and short action potentials shown in Fig. 2 suggests that I_{Ca} contributes significantly to the development of alternans. Experiments using calcium channel blockers also have indicated that I_{Ca} may mediate alternans (23). To simulate the effects of a generic calcium channel blocker in the model, we decreased the magnitude of I_{Ca} by 20%. Figure 4 shows the action potential and plateau currents in the decreased I_{Ca} model at a pacing cycle length of 180 ms. No alternans of I_{Ca} or action potential duration occurred at this or any other pacing cycle length. As expected, the restitution relation lacked a region of slope equal to 1 (Fig. 5*A*).

The elimination of alternans in the reduced I_{Ca} model was mediated primarily by alterations of calcium-induced inactivation of I_{Ca} and the resultant changes in action potential duration (Fig. 6*A*). After a long diastolic interval, calcium-induced inactivation recovered to a nearly maximal value, which resulted in a large I_{Ca} during the next action potential and a correspondingly long action potential duration. Because of the long action potential duration, the next diastolic interval was shortened. Consequently, the calcium-induced inactivation gate did not recover fully by the time the next stimulus was applied. The subsequent I_{Ca} was smaller, causing a shorter action potential duration. A long diastolic interval followed the short action potential duration, and the cycle repeated.

When I_{Ca} was diminished, the action potential duration was shortened, resulting in a prolongation of diastolic interval (Fig. 6*B*). The longer diastolic interval allowed for complete recovery of f_{Ca}. Consequently, I_{Ca} was constant for each action potential, although reduced in magnitude.

According to the scenario described above, not only should a reduction of I_{Ca} decrease alternans magnitude, but an increase in I_{Ca} should increase alternans

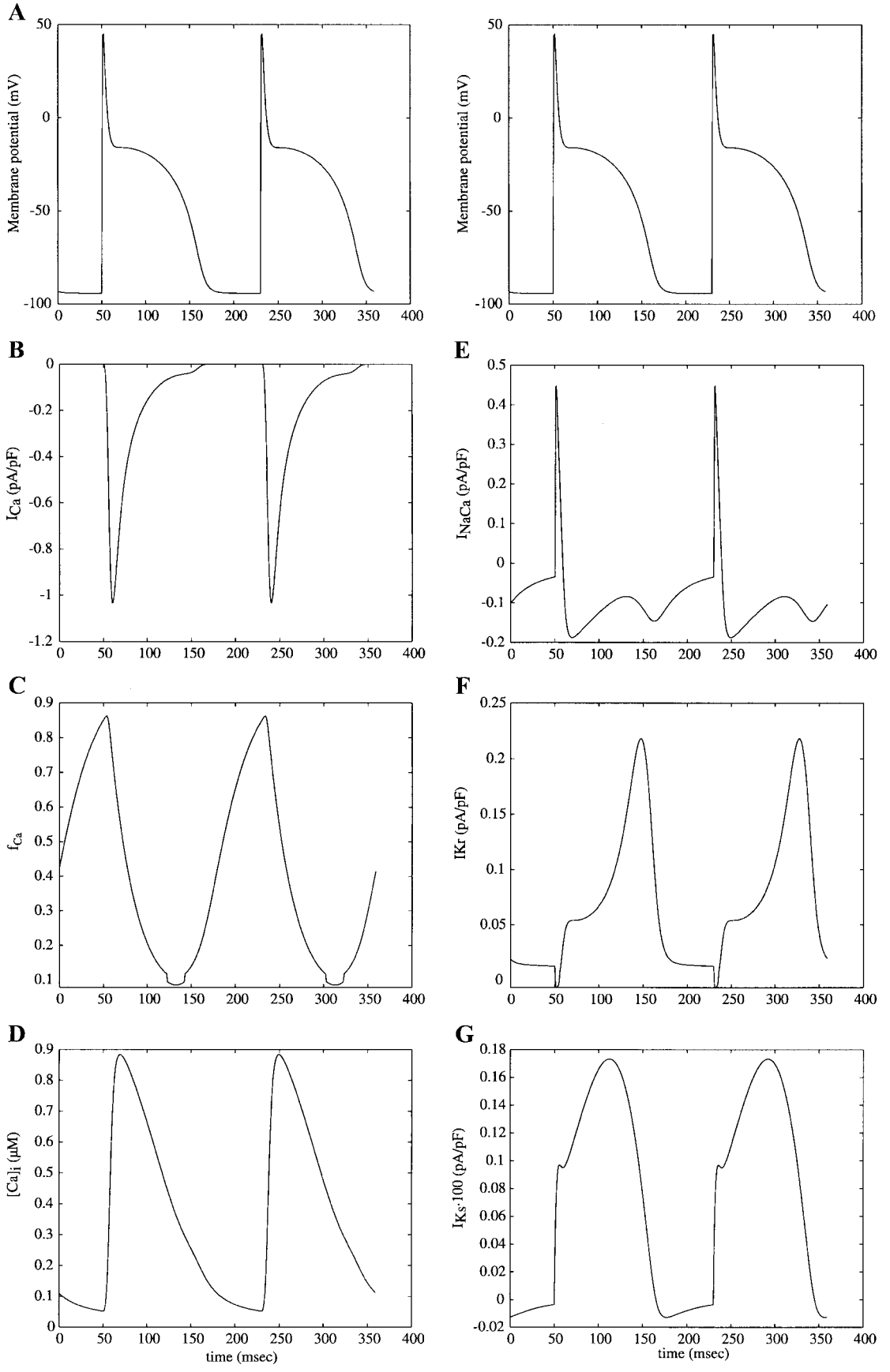

Fig. 4. Action potentials, ionic currents, and Ca^{2+} transients generated by the reduced I_{Ca} CVM model at a pacing cycle length of 180 ms. *A*: action potentials; *B*: I_{Ca}; *C*: f_{Ca}; *D*: $[Ca^{2+}]_i$; *E*: I_{NaCa}; *F*: I_{Kr}; *G*: I_{Ks}.

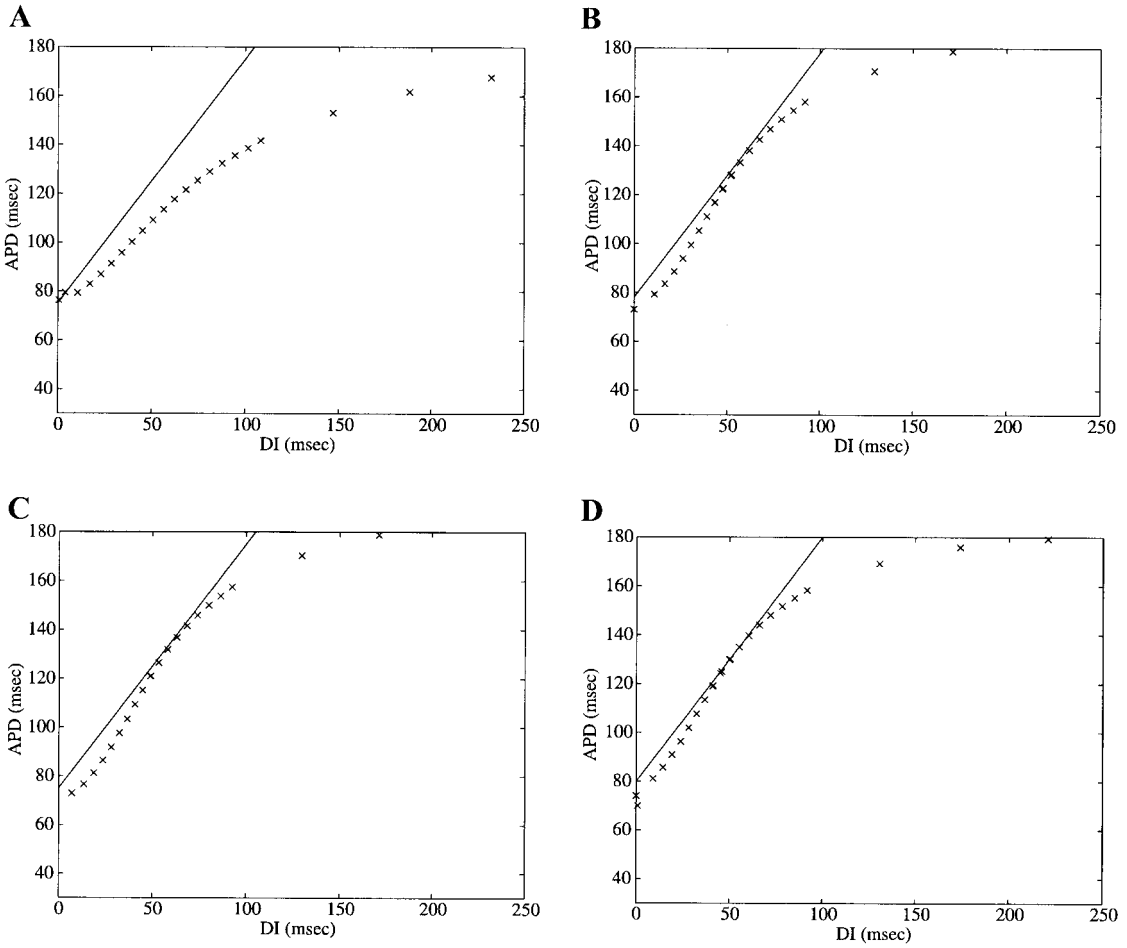

Fig. 5. Relationship between APD and DI in the CVM model after reducing $\bar{P}_{Ca}$ by 20% (*A*), increasing $\bar{G}_{K1}$ by 7% (*B*), increasing $\bar{G}_{Kr}$ by 62% (*C*), and increasing $\bar{G}_{Ks}$ by 14.3-fold (*D*). The solid line has a slope of 1. See *Glossary* for abbreviations.

magnitude. To test this hypothesis, the magnitude of I_{Ca} was varied, and the resultant magnitude of action potential duration alternans was measured. As shown in Fig. 7, alternans magnitude was proportional to the magnitude of I_{Ca}. In addition, alternans magnitude could be altered predictably by varying the time constant for calcium-induced inactivation ($\tau_{f_{Ca}}$), where decreasing $\tau_{f_{Ca}}$ eliminated alternans of I_{Ca} and action potential duration, secondary to a reduction in the magnitude of I_{Ca}, and increasing $\tau_{f_{Ca}}$ had the opposite effects.

The magnitude of action potential duration alternans also could be altered by changing the magnitude of I_{Na} and I_{NaCa} (Fig. 7). As I_{Na} was increased (by increasing $\bar{G}_{Na}$), alternans magnitude decreased. Conversely, alternans magnitude was increased after a reduction of I_{Na}. Both increases and decreases of I_{NaCa}, secondary to alterations of k_{NaCa}, reduced the magnitude of action potential duration alternans.

Role of repolarizing K^+ currents in alternans. The effects of altering I_{to}, I_{Kp}, I_{K1}, I_{Kr}, and I_{Ks} on alternans also were determined (Fig. 7). The magnitude of each of the currents was increased individually until alternans no longer occurred during pacing at any cycle length. Elimination of alternans occurred after increasing I_{to} by ≥10%, I_{K1} by ≥7%, or I_{Kr} by ≥62%. A substantially greater increase in the magnitude of I_{Ks} or I_{Kp} was required to eliminate alternans. Decreasing the magnitude each of the K^+ currents increased the magnitude of action potential duration alternans with the exception of I_{to}, where decreasing the magnitude of the current decreased the alternans magnitude.

Increasing I_{K1}, I_{Kr}, or I_{Ks} reduced action potential duration from a control value of 220 ms to 211, 211 and 197 ms, respectively, at a pacing cycle length of 1,000 ms. Despite the reduction in action potential duration, the magnitudes of I_{Ca} and the Ca^{2+} transient were minimally affected, both at short pacing cycle lengths (compare Figs. 2 and 8) and at a cycle length of 1,000 ms: peak I_{Ca} magnitudes for control and elevated I_{K1}, I_{Kr}, and I_{Ks} were −1.57, −1.57, −1.57, and −1.58 pA/pF, respectively, and peak $[Ca^{2+}]_i$ magnitudes were 2.15, 2.10, 2.12, and 2.04 μM, respectively.

DISCUSSION

We developed an ionic model of the canine ventricular muscle cell that generates physiologically realistic

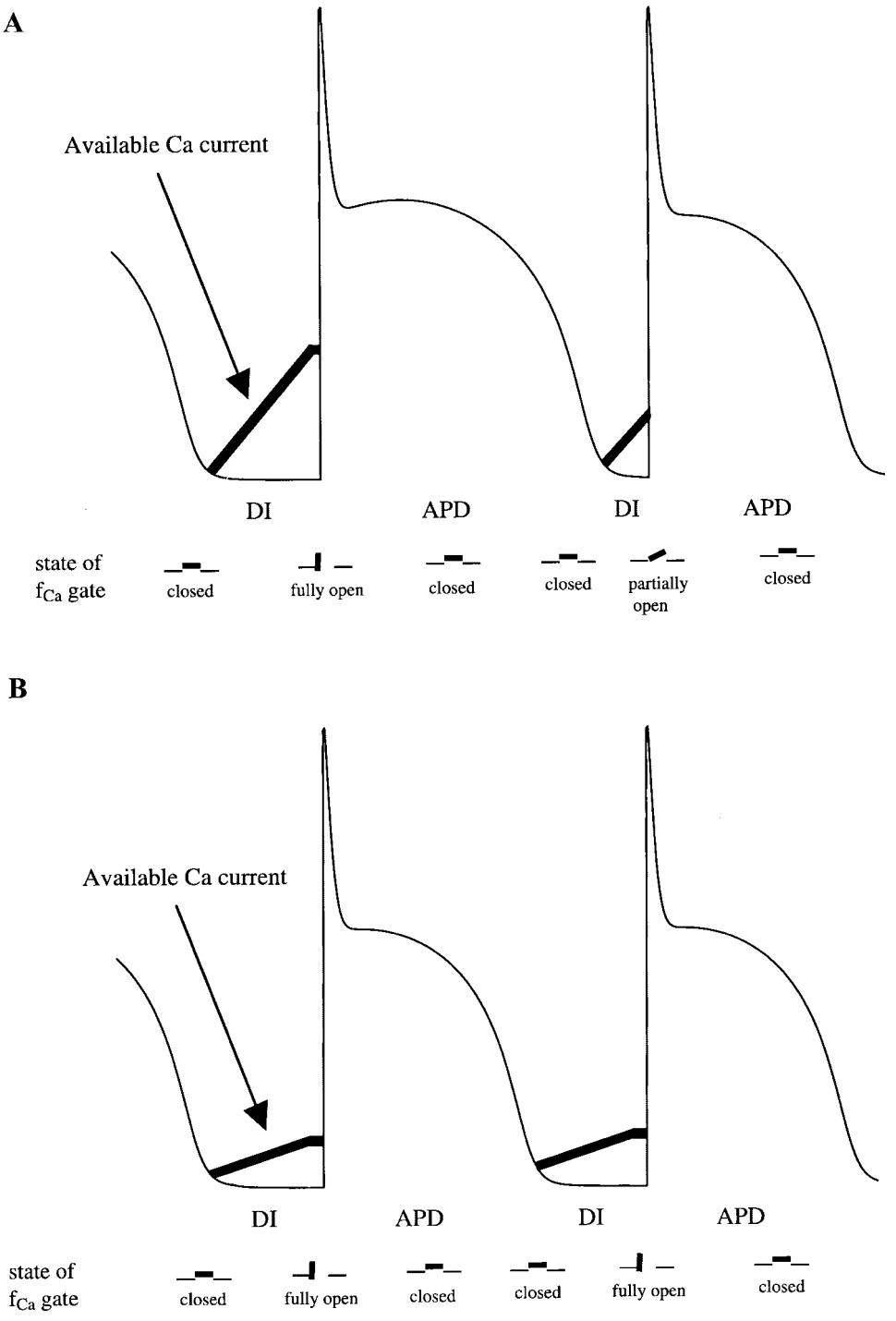

Fig. 6. Relationship among the kinetics of the calcium-induced inactivation gate (f_{Ca}), APD, DI, and the time course of I_{Ca} in the normal CVM model (*A*) and in the reduced I_{Ca} model (*B*) at a pacing cycle length of 180 ms. See text for discussion and *Glossary* for abbreviations.

action potential duration alternans characterized by a large magnitude and a wide range of pacing cycle lengths over which they appear. Action potential duration alternans was caused primarily by an alternans of I_{Ca}, where the latter resulted from the time-dependent behavior of the calcium-induced inactivation gate, f_{Ca}. Alternans was suppressed by reducing the magnitude of I_{Ca} as well as by increasing the magnitude of selected repolarizing K^+ currents. Although the CVM model has some limitations, as discussed below, it is the first ionic model of the CVM that reproduces physiological alternans at rapid pacing rates. As such, it provides a useful simulation tool for studying the complicated interactions of cardiac membrane currents.

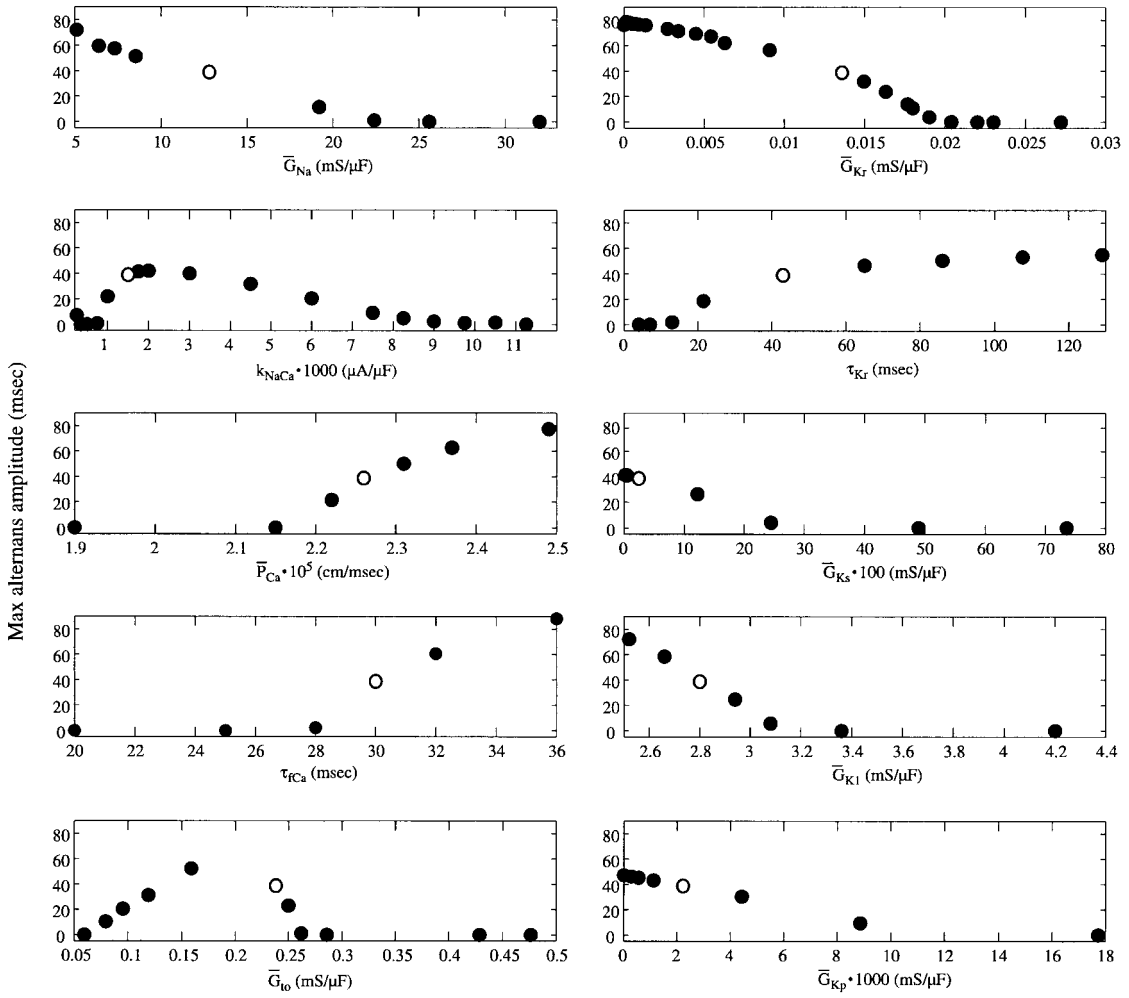

Fig. 7. Dose-response relationships between ionic current magnitude and alternans magnitude in the CVM model. Shown are the maximum magnitudes of APD alternans as a function of a particular model parameter. ○, Control parameter value. *Left* (from *top* to *bottom*): maximum I_{Na} conductance, I_{NaCa}, maximum I_{Ca} permeability, time constant for f_{Ca}, and maximum conductance for I_{to}. *Right* (from *top* to *bottom*): maximum conductance for I_{Kr}, time constant for I_{Kr}, maximum conductance for I_{Ks}, maximum conductance for I_{K1}, and maximum conductance for I_{Kp}. See *Glossary* for abbreviations.

Role of I_{Ca} in alternans. The development of action potential duration alternans required that *1*) the duration of the action potential have a sensitive dependence on I_{Ca} and *2*) the recovery of I_{Ca} have a sensitive dependence on diastolic interval. The first condition applied so long as there was a relative balance of repolarizing K^+ current and I_{Ca} during the action potential plateau. The second condition was manifest during pacing at short cycle lengths, where partial recovery of I_{Ca} after short diastolic intervals resulted in short action potential durations, followed by long diastolic intervals. Nearly complete recovery of I_{Ca} after long diastolic intervals produced action potentials with long durations, followed by short diastolic intervals. By this mechanism, a self-perpetuating sequence of long-short action potential durations was established. A similar mechanism likely contributed to action potential duration alternans in previously published ionic models (1, 22), although alternans of I_{Ca} was not specifically reported in those studies.

After the magnitude of I_{Ca} was reduced by decreasing $\bar{P}_{Ca}$ or increasing calcium-induced inactivation, the balance of I_{Ca} and repolarizing K^+ currents was shifted in favor of the repolarizing currents, resulting in shorter action potential durations. The resultant longer diastolic intervals allowed for complete recovery of I_{Ca}, albeit to a lesser magnitude, during pacing at cycle lengths that induced alternans in the control model. At even shorter pacing cycle lengths, diastolic intervals were too short to allow full recovery of I_{Ca}. However, because of the reduced magnitude of I_{Ca} and rate-dependent accumulation of incompletely deactivated K^+ current, the dependence of action potential duration on I_{Ca} was minimized and action potential durations remained consistently short. A similar mechanism accounts for the attenuation of alternans in the control model at very short pacing cycle lengths (Fig. 3).

Role of repolarizing K^+ currents in alternans. Beat-to-beat alterations of I_{K1}, I_{Kr}, and I_{Ks} appeared to play

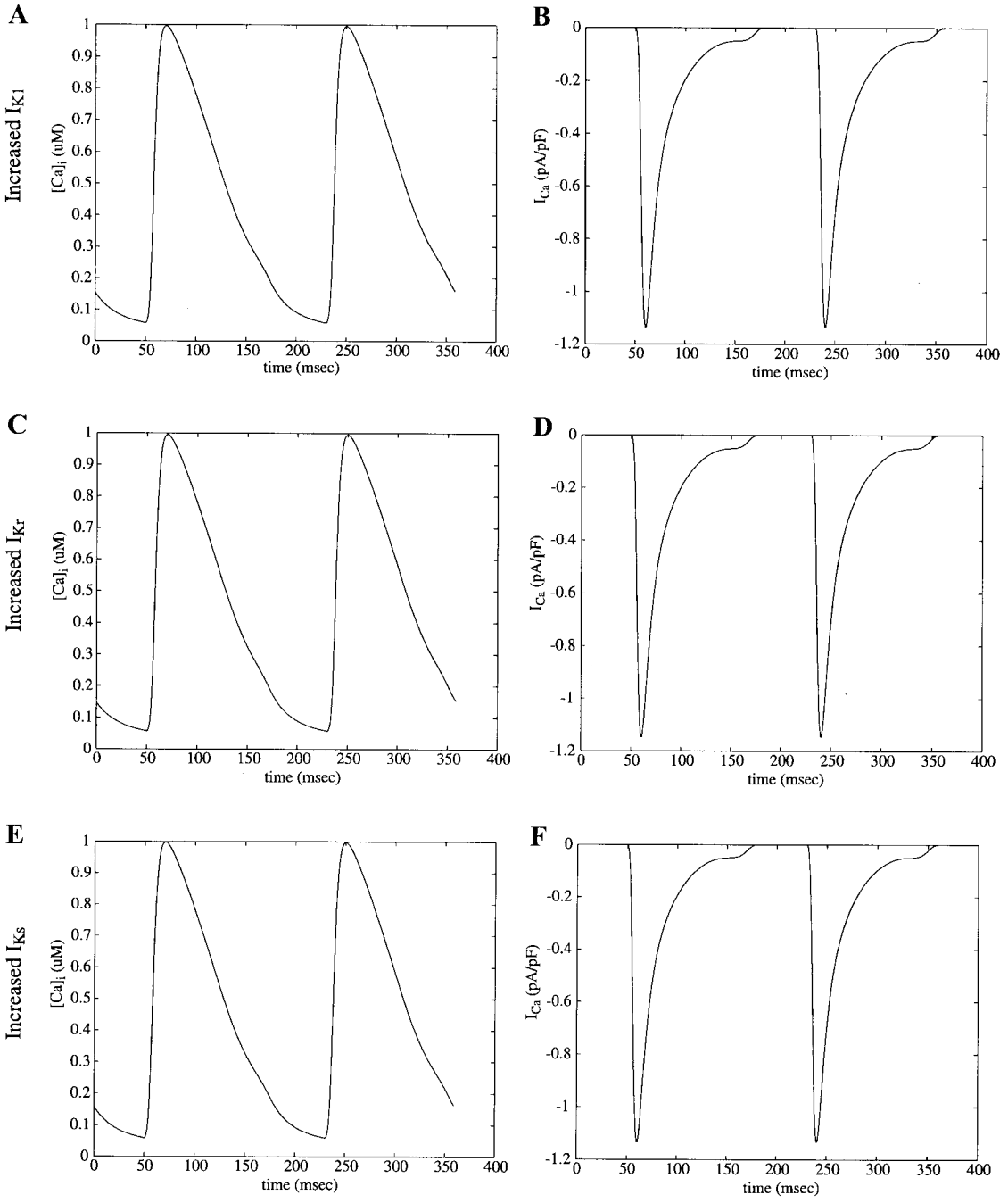

Fig. 8. $[Ca^{2+}]_i$ (*left*) and I_{Ca} (*right*) in the CVM model after increasing I_{K1} (*A* and *B*), I_{Kr} (*C* and *D*), or I_{Ks} (*E* and *F*). See *Glossary* for abbreviations.

a minor role in mediating alternans. As expected, I_{K1}, which has no time dependence, displayed no beat-to-beat variations in magnitude, whereas the beat-to-beat changes in I_{Ks} were too small to affect action potential duration appreciably at short pacing cycle lengths. Total I_{Kr} also alternated during alternans; however, peak I_{Kr} did not, suggesting that alternation of I_{Kr} resulted from alternans of action potential duration rather than vice versa.

Although the beat-to-beat variations of I_{K1}, I_{Kr}, and I_{Ks} did not contribute appreciably to alternans, increasing any one of these currents sufficiently suppressed alternans. The mechanism for this effect was analogous to that described in *Role of I_{Ca} in alternans* for the suppressant effects of reducing I_{Ca} on alternans. With elevation of I_{K1}, I_{Kr}, or I_{Ks}, the balance of repolarizing K^+ currents and I_{Ca} during the action potential plateau was skewed, resulting in consistently short action potential durations. Consequently, the pattern of action potential duration and diastolic interval was similar to that shown in Fig. 6*B* except that I_{Ca} not only recovered fully but also achieved a larger magnitude.

Implications. Decreasing the magnitude of I_{Ca}, either experimentally (23) or in an ionic model (22), has been shown to eliminate alternans and to convert VF into a periodic rhythm. However, this approach clearly is not useful clinically because decreasing I_{Ca} decreases the Ca^{2+} transient, thereby reducing contractile force. With the use of the CVM model to explore other methods for eliminating alternans, we found that alternans was suppressed by increasing the magnitude of three repolarizing K^+ currents: I_{K1}, I_{Kr}, and I_{Ks}.

Given that increasing I_{K1}, I_{Kr}, and I_{Ks} decreased action potential duration, we determined whether such shortening truncated I_{Ca}, in which case increasing K^+ conductance might have the same clinical limitation as decreasing Ca^{2+} conductance. However, I_{Ca} was minimally affected both at short and at long pacing cycle lengths, as was the Ca^{2+} transient. Consequently, it is possible, at least in the CVM model, to increase K^+ conductance to the point of suppressing alternans without reducing contractility.

These simulation results suggest a novel strategy for treating ventricular tachyarrhythmias. Previous attempts at treatment of such arrhythmias with pharmacological agents have been largely unsuccessful. In particular, class III antiarrhythmic drugs, which are designed to block K^+ currents, have been shown to be proarrhythmic (20). The CVM simulations suggest that a new class of drugs designed to increase the magnitude of selected outward currents may be useful in preventing alternans and, therefore, in preventing the development of arrhythmias such as VF. It should be emphasized, however, that only those K^+ channel agonists that reduce the slope of the action potential duration restitution relation are expected to suppress VF. Drugs such as ATP-sensitive K^+ channel current agonists, which markedly increase outward K^+ current and shorten action potential duration, increase the slope of the restitution relation and, presumably by that mechanism, facilitate the induction of VF (27).

Limitations. While the CVM model successfully reproduces alternans, it has several limitations. First, the formulation of I_{Ca} is based solely on the qualitative characteristics of I_{Ca}. To improve the model, I_{Ca} should conform to the results of quantitative voltage-clamp experiments, where the latter ideally have been conducted under circumstances that preserve the native behavior of I_{Ca} during pacing at short cycle lengths (e.g., no buffering of $[Ca^{2+}]_i$ or washout of the intracellular space). Second, although the simplified calcium handling in the model reproduces physiological Ca^{2+} transients, it ignores several of the details of calcium release from the SR. Further work needs to be done to incorporate detailed calcium handling mechanisms such as those in the Winslow model (26). Third, the model does not include the late Na^+ current, which may contribute significantly to plateau duration (28). A formulation of this current that agrees with voltage-clamp experiments also needs to be included to complete the model. Finally, it has been shown that transmural heterogeneity of the heart is caused by differences in I_{to}, I_{Ks}, I_{NaCa}, and the late Na^+ current in endocardial, midmyocardial, and epicardial canine heart cells (13, 14, 27, 29). We hope in the future to develop specific models for canine endocardium, midmyocardium, and epicardium cells that will take these differences into account.

These studies were supported by Integrative Graduate Education and Research Trainership Program in Nonlinear Systems National Science Foundation Grant DGE-9870631, by National Heart, Lung, and Blood Institute Grant HL-84536, and by a grant-in-aid from the American Heart Association, New York State Affiliate.

REFERENCES

1. **Chudin E, Goldhaber J, Garfinkel A, Weiss J, and Kogan B.** Intracellular Ca^{2+} dynamics and the stability of ventricular tachycardia. *Biophys J* 77: 2930–2941, 1999.
2. **Chialvo DR, Gilmour RF Jr, and Jalife J.** Low dimensional chaos in cardiac tissue. *Nature* 343: 653–657, 1990.
3. **Courtemanche M.** Complex spiral wave dynamics in a spatially distributed ionic model of cardiac electrical activity. *Chaos* 6: 579–600, 1996.
4. **Freeman LC, Pacioretty LM, Moise Kass RS NS, and Gilmour RF Jr.** Decreased density of I_{to} in left ventricular myocytes from German shepherd dogs with inherited arrhythmias. *J Cardiovasc Electrophysiol* 8: 872–883, 1997.
5. **Garfinkel A, Kim YH, Voroshilovsky O, Qu Z, Kil JR, Lee MH, Karaguezian HS, Weiss JN, and Chen PS.** Preventing ventricular fibrillation by flattening cardiac restitution. *Proc Natl Acad Sci USA* 97: 6061–6066, 2000.
6. **Gilmour RF Jr and Chialvo DR.** Editorial: electrical restitution, critical mass and the riddle of fibrillation. *J Cardiovasc Electrophysiol* 10:1087–1089, 1999.
7. **Gintant GA.** Characterization and functional consequences of delayed rectifier current transient in ventricular repolarization. *Am J Physiol Heart Circ Physiol* 278: H806–H817, 2000.
8. **Guevara MR, Ward G, Shrier A, and Glass L.** Electrical alternans and period doubling bifurcations. *IEEE Comp Cardiol* 562: 167–170, 1984.
9. **Jafri S, Rice JJ, and Winslow RL.** Cardiac Ca^{2+} dynamics: the roles of ryanodine receptor adaptation and sarcoplasmic reticulum load. *Biophys J* 74: 1149–1168, 1998.
10. **Karma A.** Electrical alternans and spiral wave breakup in cardiac tissue. *Chaos* 4: 461–472, 1994.
11. **Koller ML, Riccio ML, and Gilmour RF Jr.** Dynamic restitution of action potential duration during electrical alternans and ventricular fibrillation. *Am J Physiol Heart Circ Physiol* 275: H1635–H1642, 1998.
12. **Koller ML, Riccio ML, and Gilmour RF Jr.** Effects of $[K^+]_o$ on electrical restitution and spatiotemporal organization during ventricular fibrillation. *Am J Physiol Heart Circ Physiol* 279: H2665–H2672, 2000.
13. **Liu DW and Antzelevitch C.** Characteristics of the delayed rectifier current (I_{Kr} and I_{Ks}) in canine ventricular epicardial, midmyocardial, and endocardial myocytes. *Circ Res* 76: 351–365, 1995.
14. **Liu DW, Gintant GA, and Antzelevitch C.** Ionic bases for electrophysiological distinctions among epicardial, midmyocardial, and endocardial myocytes from the free wall of the canine left ventricle. *Circ Res* 72: 671–687, 1993.
15. **Luo CH and Rudy Y.** A model of the ventricular cardiac action potential. *Circ Res* 68: 1501–1526, 1991.
16. **Luo CH and Rudy Y.** A dynamic model of the cardiac ventricular action potential. I. Simulation of ionic currents and concentration changes. *Circ Res* 74: 1071–1096, 1994.
17. **Nolasco JB and Dahlen RW.** A graphic method for the study of alternation in cardiac action potentials. *J Appl Physiol* 25: 191–196, 1968.
18. **Panfilov AV.** Spiral breakup as a model of ventricular fibrillation. *Chaos* 8: 57–64, 1998.

19. **Pastore JM, Girouard SD, Laurita KR, Akar FG, and Rosenbaum DS.** Mechanism linking T-wave alternans to the genesis of cardiac fibrillation. *Circ Res* 99: 1385–1394, 1999.
20. **Peters NS, Cabo C, and Wit AL.** Arrhythmogenic mechanisms: automaticity, triggered activity, and reentry. In: *Cardiac Electrophysiology: From Cell to Bedside*. Philadelphia, PA: Saunders, 2000, p. 345–356.
21. **Press WH, Teukolsky SA, Vetterling WT, and Flannery BP.** *Numerical Recipes in C* (2nd ed.). Cambridge, UK: Cambridge University Press, 1992.
22. **Qu Z, Weiss JN, and Garfinkel A.** Cardiac electrical restitution properties and stability of reentrant spiral waves: a simulation study. *Am J Physiol Heart Circ Physiol* 276: H269–H283, 1999.
23. **Riccio ML, Koller ML, and Gilmour RF Jr.** Electrical restitution and spatiotemporal organization during ventricular fibrillation. *Circ Res* 84: 955–963, 1999.
24. **Rush S and Larsen H.** A particular algorithm for solving dynamics membrane equations. *IEEE Trans Biomed Eng* 25: 389–392, 1978.
25. **Varro A, Balati B, Iost N, Takacs J, Virag L, Lathrop DA, Csaba L, Talosi L, and Papp JG.** The role of the delayed rectifier component I_{Ks} in dog ventricular muscle and Purkinje fiber repolarisation. *J Physiol (Lond)* 523: 67–81, 2000.
26. **Winslow RL, Rice J, Jafri S, Marban E, and O'Rourke B.** Mechanisms of altered excitation-contraction coupling in canine tachycardia-induced heart failure, II: model studies. *Circ Res* 84: 571–586, 1999.
27. **Wu TJ, Yashima M, Doshi R, Kim YH, Athill CA, Ong JJC, Czer T, Trento A, Blanche C, Kass RM, Garfinkel A, Weiss JN, Fishbein MC, Karagueuzian HS, and Chen P-S.** Relation between cellular repolarization characteristics and critical mass for human ventricular fibrillation. *J Cardiovasc Electrophysiol* 10: 1077–1086, 1999.
28. **Zygmunt AC, Eddlestone GT, Thomas GP, Goodrow RJ, and Antzelevitch C.** Larger late sodium current in M cells contributes to electrical heterogeneity in canine ventricle. *Am J Physiol Heart Circ Physiol* 281: H689–H697, 2001.
29. **Zygmunt AC, Goodrow RJ, and Antzelevitch C.** I_{NaCa} contributes to electrical heterogeneity within the canine ventricle. *Am J Physiol Heart Circ Physiol* 278: H1671–H1678, 2000.